Available online at www.sciencedirect.com
ScienceDirect
Journal of Photochemistry and Photobiology A: Chemistry 188 (2007) 74–82
Journal of Photochemistry and Photobiology A:Chemistry
www.elsevier.com/locate/jphotochem

Complexation effect of γ-cyclodextrin on a hydroxyflavone derivative: Formation of excluded and included anions

J.A. Organero, L. Tormo, M. Sanz, A. Roshal [1], A. Douhal *

Departamento de Química Física, Sección de Químicas, Facultad de Ciencias del Medio Ambiente, Universidad de Castilla-La Mancha, Avda. Carlos III, S.N. 45071, Toledo, Spain

Received 27 June 2006; received in revised form 3 November 2006; accepted 24 November 2006
Available online 1 December 2006

Abstract

In this work, we report on steady-state and time-resolved picosecond measurements of the effect of γ-cyclodextrin (CD) on the UV–visible absorption and fluorescence characteristics of 4′- dimethylaminoflavonol (DMAF) in *N*,*N*-dimethyl formamide (DMF). We first show that the electronically excited DMAF in DMF undergoes an equilibrated reaction between an intramolecular charge transfer (ICT) and a tautomer (T) formed after an intramolecular proton transfer in the former. A very small amount of anion of DMAF is also found at the ground state. Upon addition of CD, the results show larger formation of anions of DMAF through H-bonding interactions inside of the CD and at its gate giving birth to inclusion and capped complexes, respectively. Both anions emit at the same regions. However, the encapsulated one has a shorter fluorescence lifetime (∼1 ns) due to the lower polarity of the caging nano-cavity when compared to DMF. Rotational times of free (97 ps) and complexed (130 and 770 ps) DMAF agree with those expected from the hydrodynamics theory and the optimized structures using PM3 calculations. The results add new information on the interaction of CD with phenol-containing probes, and it may be relevant to the design of sensors using these nano-hosts and to drug delivery field using CD.

Keywords: Absorption; Emission; Equilibrium constant; Cyclodextrin; Flavonol; Picosecond; Dynamics; Anisotropy; Inclusion; Capped; H-bond; Cooperativity

1. Introduction

Encapsulation of aromatic molecules (guests) by cyclodextrins (CD) can induce large changes in their photochemical and photophysical events [1–9]. Therefore CD nano-cavities caging has been used to study proton-transfer reactions, twisting motion, formation of an excimer and reaction rates. In a previous contribution, we reported on the caging effect of γ-CD on 3-hydroxyflavone (3HF) [10]. The result shows a stabilization of the caged anion of 3HF in the ground state, due to a cooperative H-bonding network effect of the nano-cage. Other works showed the presence of the anion structure of 3HF when caged in the bovine serum albumin protein, and in alcoholic solvents [11,12]. Recent studies of 3-HF and its derivative Fisetin in aqueous solutions of CD have reported an enhanced relative emission of the tautomer T, the structure which is formed after an ultrafast excited-state intramolecular-proton transfer (ESIPT) reaction in the enol (E) one, upon addition of CD [13,14]. The result was explained in terms of reducing intermolecular interactions of the dyes with water due to the caging effect of CD, and making, thus, more favourable the ESIPT in the included dye [13,14].

On the other hand, several studies have been done on 4′-dialkylaminoflavonol derivatives, and show remarkable solvent effect (mainly due to the polarity) on the result of their ESIPT reactions [15–21]. These molecules exhibit two emission bands. One corresponds to the emission of an intramolecular charge-transferred (ICT) structure and the other one corresponds to the proton transferred tautomer (T) [22–27]. In nucleophilic and apolar solvents the intramolecular proton-transfer process is irreversible, while it is reversible for non nucleophilic polar solvents. Thus, upon increasing the solvent polarity, the equilibrium shifts toward the ICT state possessing a large dipole moment with respect to the T structure [18,19]. In 4′-diethylaminoflavonol the dipole moment of excited ICT (9.21 D) is significantly

* Corresponding author. Fax: +34 925 268840.
E-mail address: Abderrazzak.douhal@uclm.es (A. Douhal).
[1] Permanent address: Department of Physical Organic Chemistry, Institute of Chemistry at Kharkov National University, 4 Svobody sqr., Kharkov 61077, Ukraine.

1010-6030/$ – see front matter © 2006 Elsevier B.V. All rights reserved.
doi:10.1016/j.jphotochem.2006.11.022

larger than that of excited T (5.5 D) [18]. The result suggests the existence of a competition between solvent relaxation and proton transfer process. 4′-dimethylaminoflavonol (DMAF) is a derivative of 3HF, but it exhibits a different behaviour in the excited state. Recently, we reported on a femtosecond (fs) time-resolved fluorescence study of DMAF in solution [15]. We showed that the excited enol form undergoes an ultrafast intramolecular charge-transfer (ICT) process at S_1 induced by the dimethyl-amino group followed by an ESIPT reaction to give a keto tautomer (T). In apolar solvents, the ICT reaction is not favourable and the ESIPT is abnormally slow (∼2 ps) and irreversible. However, for highly polar solvents, the ICT reaction in E is very fast (∼100–200 fs) to give an ICT state, and a subsequent T in equilibrium with its precursor (ICT).

In the present work, we focus on the caging of DMAF by γ-CD in *N*,*N*-dimethyl formamide (DMF) solution, and we show the cooperativity effect of OH-groups of γ-CD in stabilizing the formed anionic complexes of 1:1 stoichiometry. Steady-state and ps-time resolved experiments together with theory were used to elucidate the nature of the complexes and their photodynamics.

2. Experimental and theoretical methods

DMAF was synthesized using Algar-Flynn-Oyamada reaction and it was purified by means of a repeated recrystallisation from methanol solutions [28]. γ-CD (from Sigma–Aldrich) was used as received. Anhydrous DMF (Sigma–Aldrich, 99.8%) was used after drying and purification by standards methods. Steady-state absorption and emission spectra were recorded on a Varian (Cary E1) and Perkin-Elmer LS 50B spectrophotometers, respectively. Excited-state emission lifetimes were measured by using a time-correlated single-photon counting picosecond spectrophotometer (FluoTime 200). The sample was excited by a pulsed laser centred at 393 or at 433 nm. The instrumental response function (IRF) was typically 65 ps. The emission signal was collected at the magic angle. The emission decay data were convoluted with the IRF signal and fitted to a multi-exponential function using the Fluofit package. The quality of the fits was characterized in terms of residual distribution and reduced χ^2 value. Details on the apparatus and procedure of data analysis were described [9]. All the measurements were done at 293 ± 1 K.

Quantum calculations to find the most stable guest–host complexes were performed using the GAUSSIAN 03 software package [29]. The γ-CD molecule was optimized by PM3 method from the crystal structure (Cambridge structure data base). The glycoside oxygen atoms of the largest gate of CD were placed into an XY plane containing the gate, and their centres were defined as the centre of the coordination system. DMAF molecule was initially placed along the *Z* axis passing from the centre of CD and through its long axis. The position of the guest was determined by the *Z* coordinate of its centre of mass. The geometry of the guest–host complex was completely optimized by PM3 without any restriction. Therefore, we have considered three kinds of complexation modes to form the complexes. A mode for which the inclusion of DMAF into γ-CD is through the phenyl-amino part, a second one for which the process of inclusion is through the chromone moiety, and the third one in which the longer dimension of DMAF was placed parallel to the largest gate of CD (XY plane).

3. Results and discussion

3.1. Steady-state absorption and fluorescence spectra

Fig. 1A shows the UV–visible absorption spectra of $\sim 10^{-5}$ M DMAF in solutions of DMF having different concentrations of γ-CD. These spectra have the maximum intensity at ∼400 nm, a band which corresponds to the absorption of the enol (E) structure. It is clear that addition of γ-CD gives birth to a new band at ∼475 nm, and to a decrease of the E one. The band at 475 nm is explained in terms of the formation of a stabilized anion (A) of DMAF through strong H-bond interactions with γ-CD leading to the shift of the proton of the DMAF OH group to CD, as it has been reported for its parent molecule 3HF [10]. This explanation is supported by the result of adding a small amount of solid NaOH to the DMAF/DMF solution, and which provokes the disappearance of E band to give a new strong one having the maximum at ∼475 nm (not shown). Thus, this new band is clearly due to the absorption of A. For CD solution, a clear isosbestic point at 423 nm reveals the existence of equilibrium between the E and A structures.

Fig. 1A shows the effect of adding 1.7 M of water to a DMF solution of DMAF in presence of 110 mM of γ-CD. The figure also exhibits the effect of adding 100 mM of dried maltose (two linked glucose units lacking a hydrophobic nano-cavity but having eight OH groups) to the same solution of DMAF. In the first sample, we observed a small decrease (∼10%) of the 475 nm absorption band intensity. We explain the result in terms of a protonation of A to give E, and probably due to a weak exclusion of A from γ:CD cavity caused by the interactions with water molecules located at the gate of CD. For the effect of maltose in the second sample, we observed a small increase in the anionic band intensity (∼15%). This change is not large as the one induced by γ-CD, but it is enough significant to suggest the interaction of DMAF with γ-CD glucopyranose units without inclusion.

Therefore, the increase in the absorption band intensity at ∼475 nm upon addition of γ-CD is a consequence of the formation of anionic complexes with γ-CD, and not because of the hydration of the host. The change in the absorption band in presence of γ-CD reveals a significant interaction between the guest and the host. In the formed entities, the H-bond interaction provokes deprotonation of the OH group of DMAF and formation of its anionic forms, which might be included (inclusion complex, A_{in}: γ-CD) or not (capped complex, A_{out}: γ-CD). We explain the energetic balance in favour of anion formation of DMAF as a result of a cooperative effect of the 16 OH groups at the largest gate of the γ-CD nano-cavity [10].

To describe the above complexes formation of DMAF with γ-CD, we considered the following equilibria:

$$E + \gamma\text{-CD} \overset{K_1}{\rightleftarrows} A_{in} : \gamma\text{-CD} \quad (1)$$

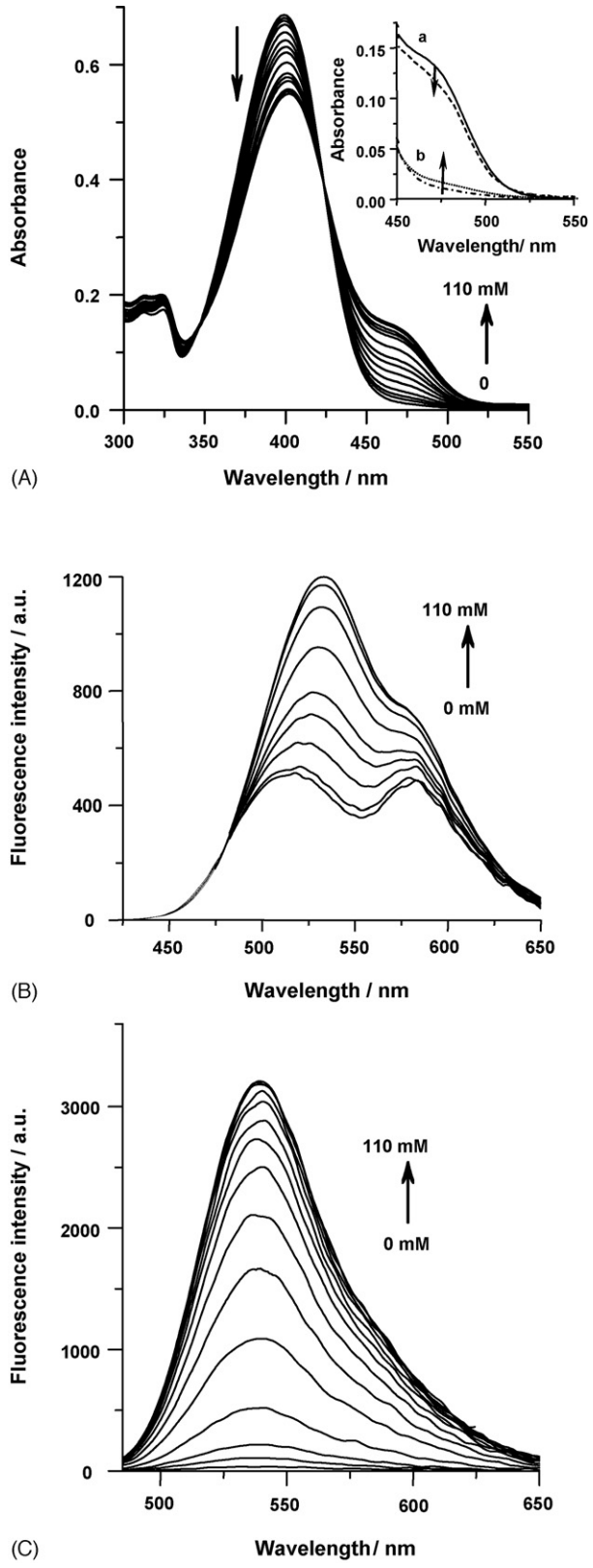

Fig. 1. UV–visible (A) absorption and (B and C) emission spectra of 4′-dimethylaminoflavonol (DMAF) in *N*,*N*-dimethylformamide (DMF) at different concentrations of γ-CD. The inset shows the weak effect of (a) addition of 1.7 M of water on the 475 nm absorption band of DMAF in DMF with of 110 mM of γ-CD solution and (b) addition of 100 mM of maltose to a DMAF in DMF solution. For (B and C) the excitation wavelengths were 390 and 475 nm, respectively.

$$E + \gamma\text{-CD} \overset{K_2}{\rightleftarrows} A_{\text{out}} : \gamma\text{-CD} \tag{2}$$

where A_{in}:γ-CD and A_{out}:γ-CD refer to the inclusion (A_{in}) and capped (A_{out}) complexes of *A* and γ-CD, respectively (Fig. 2A).

(1) and (2) give the apparent equilibrium (3) in which A_{bound} states for both inclusion and capped complexes:

$$E + \gamma\text{-CD} \overset{K_{\text{app}}}{\rightleftarrows} A_{\text{bound}} \tag{3}$$

The apparent equilibrium constant (K_{app}) is given by:

$$K_{\text{app}} = \frac{[A_{\text{bound}}]}{[E][\gamma\text{-CD}]} \tag{4}$$

The treatment of the experimental data to obtain the value of K_{app} has been previously described [30], and it consists in fitting the data by the following equation:

$$\Delta A = K_{\text{app}} \frac{\Delta a [\text{DMAF}]_0 [\gamma\text{-CD}]_0}{1 + K_{\text{app}} [\gamma\text{-CD}]_0} \tag{5}$$

where ΔA refers to the difference between the absorption intensity in absence and presence of γ-CD. The subscript "0" denotes the total concentration, and Δa is the maximum value of ΔA. Fig. 2B shows the variation of ΔA value at 475 nm with $[\gamma\text{-CD}]_0$ and the fit using Eq. (5). The obtained K_{app} value is $38 \pm 4\ \text{M}^{-1}$ at 293 K. This value is not very different from that reported for 3HF with γ-CD ($48\ \text{M}^{-1}$) [10].

Fig. 1B shows the emission spectra of DMAF in DMF and in presence of γ-CD when exciting at 390 nm (enol band). In pure DMF, the emissions of ICT and T are at ∼520 and ∼580 nm, respectively. Upon addition of γ-CD, the global emission intensity increases, and the shape of the spectrum changes and shifts to the red side of the spectrum by ∼8 nm. This change is a consequence of an increase in the population of the anionic structures of DMAF when complexed to γ-CD at S_0. Addition of γ-CD produces and stabilizes A, and therefore it decreases the population of E. Consequently, the photoformation of ICT and T populations decreases at S_1.

In pure DMF, when exciting at 475 nm (into the A band, Fig. 1C) we observed a weak emission band having the maximum at ∼540 nm. This band is attributed to A. Upon γ-CD addition, the fluorescence band of A gradually increases due to the formation of inclusion and capped complexes. It is worthy to note that we did not observe any shift in A emission when increasing γ-CD concentration. These results indicate that both included and capped anions of DMAF emit at the same spectral region.

3.2. Picosecond time-resolved emission study

To get information on the photodynamics of DMAF in pure DMF and in presence of γ-CD, we recorded ps-emission decays of these solutions. Fig. 3A shows the decays in pure DMF upon excitation at 393 nm (E domain) and observed at 470 and 660 nm. At these wavelengths of observation the decays of ICT and T are selectively gated and they fit to a bi-exponential function having time constants of $\tau_1 \sim 59$ and $\tau_2 \sim 234$ ps, respectively (Table 1). Moreover, the two pre-exponential factors describing

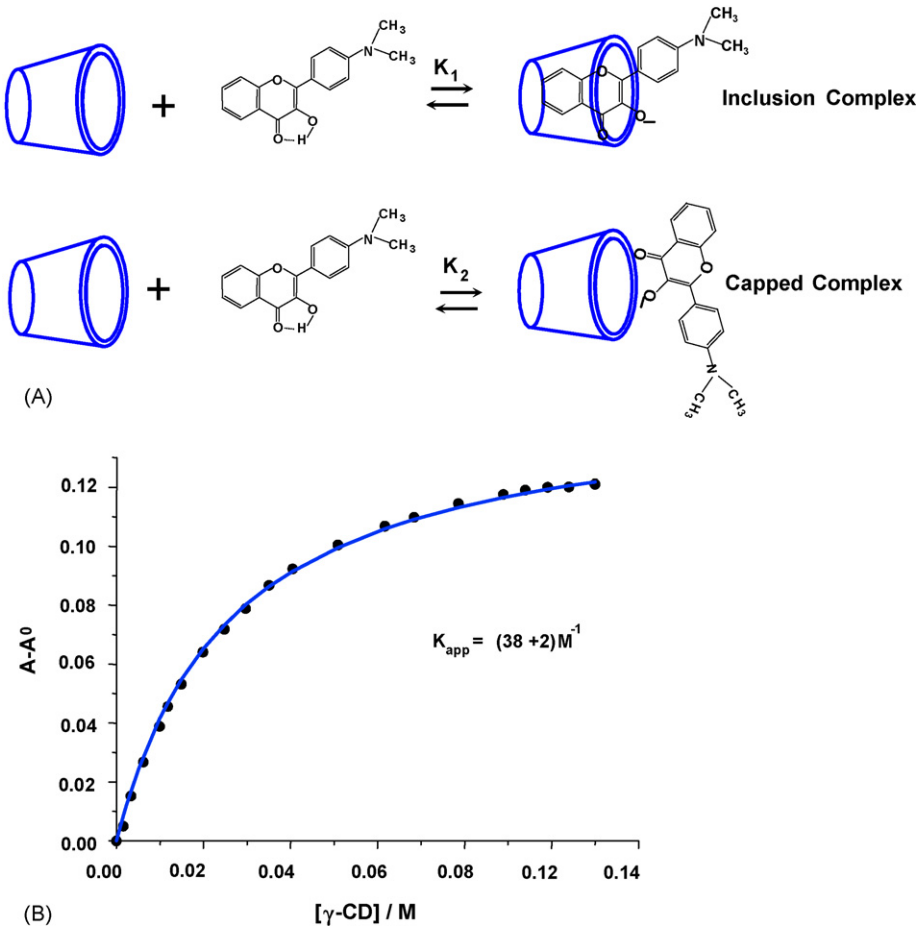

Fig. 2. (A) Variation of the absorption intensity difference ($A - A_0$) at 475 nm of DMAF upon addition of γ-CD. A_0 is the absorption intensity in absence of γ-CD. The solid line is the result of a fitting model which assumes an 1:1 stoichiometry of the formed complexes. (B) Schematic representation of the equilibria between free DMAF, γ-CD and their inclusion and capped complexes.

the growth and decay of T at 660 nm are identical in magnitude but opposite in sign. These features indicate that the ESIPT reaction connecting the ICT and T structures in DMF is reversible. Both species are equilibrated at S_1. Therefore, we analyzed the data shown in Table 1 according to the Birks model [31]. To determine the forward and back rate constants it is necessary to know the emission lifetime of ICT or T. Since these values cannot be directly obtained, we used the emission lifetime of a model molecule, where ESIPT is not possible to obtain the lifetime of ICT. The emission lifetime (0.65 ns) of the complexes of DMAF to methanol (<0.01%, v/v) in DMF was used [16]. Breaking the intramolecular H-bond in DMAF leads to formation of intermolecular ones with methanol. It produces a new component in the emission decay, and it corresponds to the open enol form of DMAF having an emission lifetime of 0.65 ns. This value was used for the determination of direct and reverse rate constants between ICT and T in DMF. Thus, operating as previously [16], we obtained the values of $9.2 \times 10^9\ s^{-1}$ and $5.1 \times 10^9\ s^{-1}$ for the rate constants of direct and reverse proton transfer processes in ICT ⇆ T. The related equilibrium constant (K) at the excited state is ∼1.8 and $\Delta G^0 = -1.42$ kJ/mol at 293 K. The values of direct and reverse proton transfer of the dye in DMF are close to those obtained in acetonitrile ($1.4 \times 10^{10}\ s^{-1}$ and $7.1 \times 10^9\ s^{-1}$) [16], a solvent which is not different from DMF as the polarity is concerned.

Table 1
Fitting values for emission decays of DMAF in pure DMF at different observation wavelengths when exciting at 393 and 433 nm

λ_{EXC} = 393 nm					λ_{EXC} = 433 nm					
λ_{em} (nm)	τ_1 (ps)	a_1 (%)	τ_2 (ps)	a_2 (%)	τ_1 (ps)	a_1 (%)	τ_2 (ps)	a_2 (%)	τ_3 (ns)	a_3 (%)
470	60	60	230	40	66	58	230	42	–	–
540	68	49	230	51	68	49	227	50	3.2	1
600	60	−44	230	56	66	−43	224	56	3.1	1
630	58	−46	238	54	66	−45	230	54	3.3	1
660	59	−50	237	50	65	−46	230	53	3.1	1

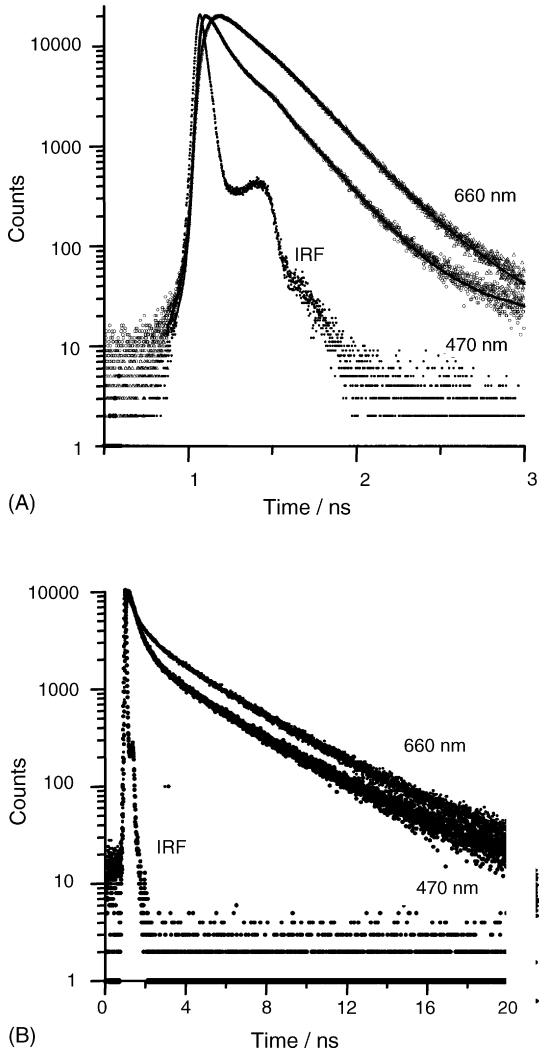

Fig. 3. Emission decays (magic angle) of DMAF in DMF at 470 and 660 nm (A) without γ-CD and exciting at 393 nm, and (B) in presence of 110 mM of γ-CD and exciting at 433 nm. IRF is the instrument response function (∼65 ps). The values of lifetimes and pre-exponential factors are given in Tables 1 and 2.

To get more information on these processes, we excited at 433 nm (close to the maximum of absorption band of A, Table 1). The decays are not shown, but Table 1 contains the fitting decays parameters using a three exponential model and which gives lifetimes of $\tau_1 \sim 60$ ps, $\tau_2 \sim 230$ ps and $\tau_3 \sim 3.2$ ns. Although the contribution of the ns-component is small (∼1%), it was necessary to introduce it to obtain an accurate fit. The shortest time (∼60 ps) are obtained in the decaying and rising components at the blue and red regions, respectively. Their relative contributions change when exciting at 393 nm (Table 1). The ns-component is assigned to the emission of A formed by a proton-transfer reaction from DMAF to DMF in the H-bonded E form. A similar process was also observed for the parent 3HF in DMF [32]. Therefore, the fluorescence of A mainly comes from the excited structure initially pumped from S_0. However, a small population of A could be formed at S_1 due to an intermolecular proton transfer reaction between the H-bonded E and DMF. This reaction may happen in few ps (<5 ps) as it occurs in 3HF/DMF solutions [32].

In presence of γ-CD and exciting at 393 nm, we could not resolve properly the contribution of anionic species because at this excitation wavelength the population of A is very low. The obtained time constants are $\tau_1 \sim 50$ ps, $\tau_2 \sim 260$ ps, $\tau_3 \sim 620$ ps and $\tau_4 \sim 2.5$ ns. When exciting at 433 nm (close to the maximum of A absorption band, Fig. 1A) a four-exponential function was needed to fit the experimental data (Fig. 3B). The obtained time constants are $\tau_1 \sim 50$ ps, $\tau_2 \sim 280$ ps, $\tau_3 \sim 1$ ns and $\tau_4 \sim 3.6$ ns (Table 2). The value of the amplitudes of these components depends on γ-CD concentration (Table 2). The components giving τ_1 and τ_2 are assigned to ICT and T emission decays, respectively. Taking into account that the amplitudes (a_3 and a_4) for τ_3 and τ_4 components are maxima when the emission decay is recorder at 540 nm (anion emission region), we assigned these components to different complexes between A and γ-CD. The presence of the 3.6 ns component (τ_4), which it is very close to that obtained in pure DMF (3.2 ns), suggests the existence of a complex in which CD does not involve its caging effect on the lifetime value, but it is H-bonded to DMAF (capped complex, Fig. 2A). A similar complex formation was proposed for Nile Red with γ-CD [33]. On the other hand τ_3 (1.1 ns) can be assigned to the caged A in 1:1 complex (inclusion complex, Fig. 2A). The protection of A by γ-CD leads to a decrease in the lifetime of the anion from ∼3.6 ns to ∼1 ns. This shortening in lifetime can be explained by considering that the interior of CD is less polar than DMF [33]. The difference in polarity should affect the rate constants of the non-radiative channels as the charges within the complex should be stabilized by a polar medium. On the other hand, the values of τ_3 are close to that recorded for the anion in dioxane (∼0.64 ns), a solvent similar to CD from the point of view of polarity [1–3]. In addition to the above assignment of the four components to fit the decays of the complexes, the heterogeneity of CD samples giving rise to inclusion complexes of different angle of inclusion and to different capped structures may lead to a large distribution of the formed entities and therefore the decays of the populations of the emitters fit a multi-exponential model.

Table 2
Fitting values for emission decays of DMAF in DMF in presence of different concentrations of γ-CD, upon excitation at 433 nm and observation at 540 nm

[γ-CD] (mM)	τ_1 (ps)	a_1 (%)	τ_2 (ps)	a_2 (%)	τ_3 (ns)	a_3 (%)	τ_4 (ns)	a_4 (%)	a_4/a_3
0	60	48	233	51	–	–	3.2	1	–
4	50	45	233	52	1.1	1	3.6	2	2.0
10	53	40	245	51	1.1	3	3.6	6	2.0
30	61	35	265	47	1.2	5	3.7	13	2.6
50	58	27	265	46	1.1	8	3.7	19	2.4
110	58	14	280	45	1.1	14	3.7	27	1.9

We now use the time-resolved data together with the absorption one (K_{app}) to have the equilibrium constant value for each complex formation. First of all, we suppose that both capped and caged anion structures have similar radiative rate constants (k_r), and thus taking into account the Strikler and Berg equation, they should have similar molar absorption coefficients (ε) [34]. Obviously, the non-radiative rate constants (k_{nr}) might be different.

The ratio between the emission quantum yields of A_{out} (capped) and A_{in} (included) entities (ϕ_{out}/ϕ_{in}) is similar to the ratio of their lifetimes (τ_{out}/τ_{in}):

$$\frac{\tau_{out}}{\tau_{in}} = \frac{\phi_{out}}{\phi_{in}} \tag{6}$$

In addition to that, the emission intensity (I_i) observed in the steady-state measurement is related to the time-resolved emission data by:

$$I_i = \frac{a_i \tau_i}{\sum_j a_j \tau_j} \tag{7}$$

$$I_i \propto \varepsilon_i \phi_i [i] \tag{8}$$

So, assuming that $\varepsilon_{out} = \varepsilon_{in}$,

$$\frac{I_{out}}{I_{in}} = \frac{a_{out}\tau_{out}}{a_{in}\tau_{in}} = \frac{\phi_{out}[A_{out}]}{\phi_{in}[A_{in}]} \tag{9}$$

Taking into account Eqs. (6), (1) and (2), we obtain:

$$\frac{[A_{out}]}{[A_{in}]} = \frac{a_{out}}{a_{in}} = \frac{K_2}{K_1} \tag{10}$$

Thus, the ratio between the amplitudes of the lifetimes of A_{out} and A_{in} (a_{out}/a_{in}) is similar to the ratio between K_2/K_1. Table 2 shows that the ratio between the amplitudes of a_4/a_3 (a_{out}/a_{in}) varies between 1.9 and 2.6. Taking into account the error in determining the a_i values when fitting the data using a multi-exponential model, we used the mean value of this ratio (2.2), and we obtained $K_2 = 2.2K_1$. Using $K_{app} = K_1 \times K_2$, we got $K_1 = 4.1\,M^{-1}$ and $K_2 = 9.3\,M^{-1}$. This result shows that the capped complex is more stable than the inclusion one by ~2.1 kJ/mol at 293 K. This energy difference might be attributed to the highest polarity of DMF compared to that of CD. The DMAF molecule outside of CD nano-cage could take any convenient position to give birth to *A*, whereas, the location of DMAF inside the CD is limited by the cavity size and shape. In addition to this geometry difference, a polar medium (DMF) stabilizes more a created charge separation in the formed complex. Other specific factors like H-bonding interactions involving the cooperativity of the OH groups of CD to stabilize the formed capped complex will be examined in the theoretical part (vide infra).

To get a clear picture of the spectral evolution of emission with time, Fig. 4 shows time-resolved emission spectra (TRES) of DMAF in DMF and in presence of 110 mM γ-CD. In pure DMF, at early times (<50 ps) we observed the emission of ICT and T structures. The relative intensity of the latter increases when time proceeds, and it reaches its maximum at about 100 ps. After this time, there is no significant change in the shape of the two bands, but a simultaneous decrease in

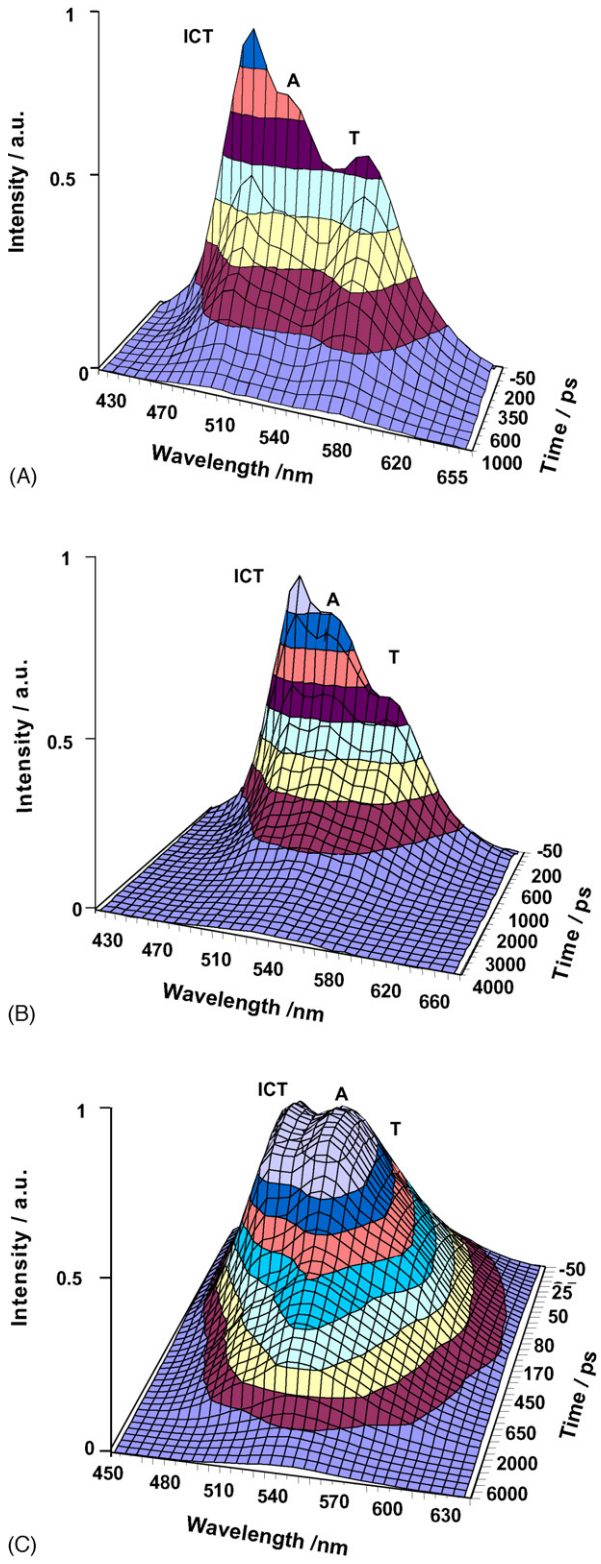

Fig. 4. Time-resolved emission spectra of DMAF (A) in pure DMF and (B) in presence of 110 mM of γ-CD upon excitation at 393 nm, and (C) in presence of 110 mM of γ-CD upon excitation at 433 nm.

intensity is observed for both, and their ratio is close to the corresponding one observed in the steady-state spectrum. These results provide an additional demonstration that the intramolecular proton-transfer reaction occurs in a time shorter than 100 ps and the existence of an equilibrium between the ICT and T forms, as the relative intensities between blue and red bands remain constant after 100 ps. An analysis of the data gave ∼110 ps as time constant for the direct proton-transfer reaction in ICT to give T. We also observed the emission of A as a shoulder at 540 nm. Fig. 4B and C show that when the solution contains γ-CD the shape of the TRES depends on the gating time. Before 100 ps, the major emission comes from ICT (510 nm), and a significant contribution from A emission is detected at 540 nm. The T emission has the maximum around 580 nm. At 200 ps the intensity of ICT band decreases, while those of A and T increase and the global emission becomes broader. At longer times (>500 ps), the spectrum is dominated by the emissions of A having lifetimes in the ns-regime.

3.3. Theoretical calculations

To have structural information on the DMAF:γ-CD complexes, we performed PM3 calculations. Though PM3 has been successfully used previously to CD chemistry [35,36], it should be noted that the theoretical results from these calculations should be considered as an approximation.

The obtained data suggest three possible complexation modes. For the inclusion entities, one fitting mode encapsulates the chromone moiety into the cavity (C_1), while the other one does it through the phenyl-amino part (C_2). To characterize these inclusion ways, we defined an inclusion angle (θ) as the angle between the plane of the embedded moiety and that perpendicular to the gate of CD. We found $\theta \sim 45^\circ$ and $\sim 10^\circ$ for the first and second inclusion modes, respectively. Furthermore, for C_1 and C_2 a length of ∼5.5 and ∼8 Å of the molecule is exposed outside of cyclodextrin, respectively. However, within C_1 the guest is more protected from the solvent effect. For the third complexation mode giving a capped complex (C_3), the long axe of DMAF was located parallel to the plane defined by the largest gate of the cavity (with 16 hydroxyl groups) and the C–O–H and C=O groups point toward the 16 OH of the largest gate.

We found that the inclusion of DMAF through the chromone moiety (C_1) gives the most stable inclusion complex, by a difference of ∼10 kJ/mol relatively to the one through the phenyl-amino moiety (C_2). However, the capped complex (C_3) is slightly more stable than C_1 by 4.2 kJ/mol. Fig. 5 exhibits the optimized structures of C_1, C_2 and C_3. The complex C_1 shows the formation of only one intermolecular H-bond ($d \sim 1.8$ Å)

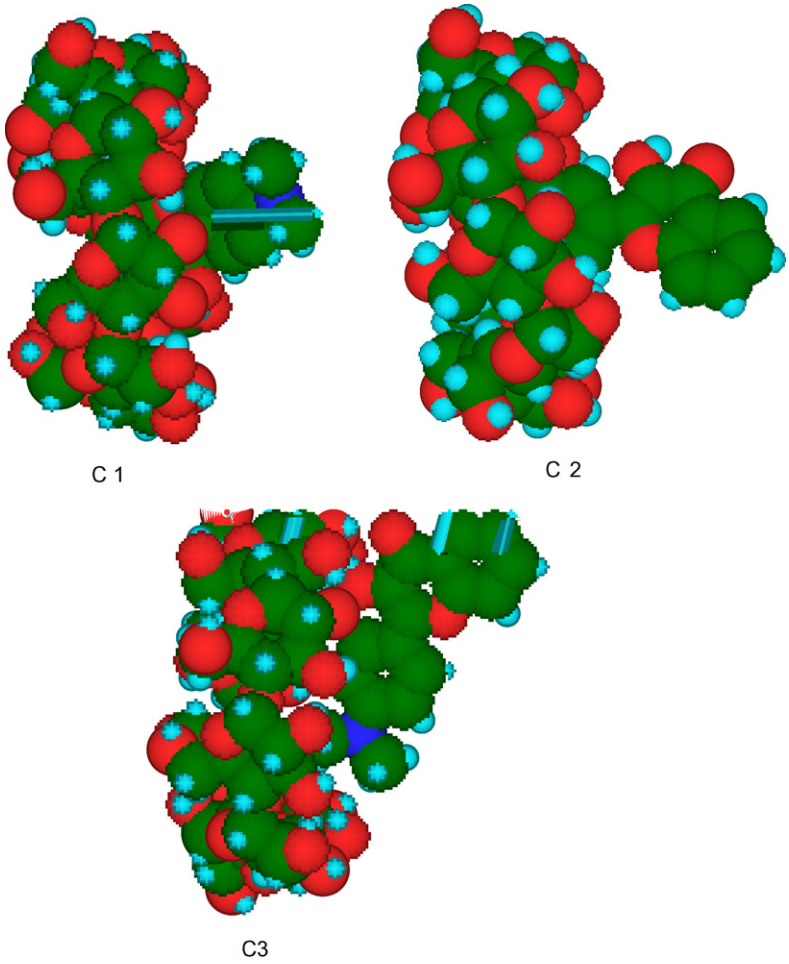

Fig. 5. Structures of the optimized 1:1 inclusion (C_1 and C_2) and capped (C_3) complexes of DMAF: γ-CD using PM3 method.

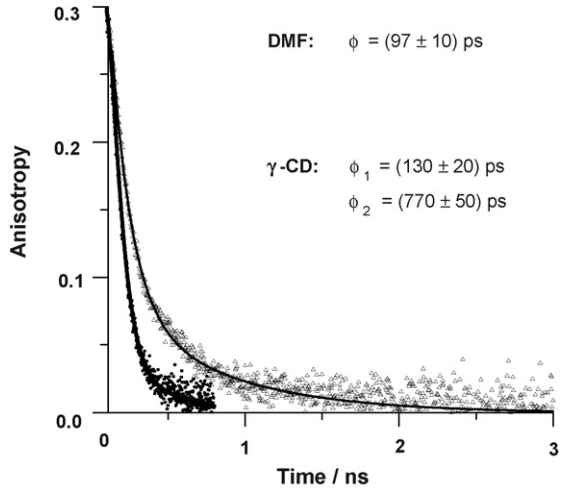

Fig. 6. Emission anisotropy ($r(t)$) decays of DMAF (●) in pure DMF and (△) in presence of 110 mM of γ-CD. Excitation and emission wavelengths were 433 and 540 nm, respectively. The solid curves are from the fits.

between an OH of γ-CD and the C–O–H group of DMAF. For C_3, we observed the formation of an intermolecular H-bond ($d \sim 1.8$ Å) between the C=O group of DMAF and an OH of γ-CD, and two intermolecular H-bonds (∼1.8 Å) between C–O–H and two OH of γ-CD. The formed three intermolecular H-bonds in C_3 helped by the cooperative H-bonding network of γ-CD favour the ionization of DMAF and stabilize the capped complex. The polarity of the solvent will then contribute to its stabilization as we experimentally observed.

3.4. Picosecond time-resolved emission anisotropy

To elucidate the dynamics of the orientational motion of DMAF and of the guest–host systems, we measured the rotational relaxation times (ϕ) of the emitters using time-resolved fluorescence anisotropy ($r(t)$) technique. Representative $r(t)$ decays are shown in Fig. 6 upon excitation at 433 and emission at 540 nm. To begin with DMAF in pure DMF, the decay of $r(t)$ at any observation wavelength from 470 to 660 nm fits to a mono-exponential function of time constant $\phi \sim 97 \pm 10$ ps (∼100 ± 10 ps when exciting at 393 nm). A comparable rotational time (85 ps) has been observed for its parent molecule 3HF [10].

Modelling DMAF as a prolate ellipsoid (an ellipsoid of revolution formed by rotation about its major axis) non-hydrated rotor, and using the hydrodynamics theory [37,38] (Eq. (12)), we calculated the rotational time of DMAF in DMF.

$$\phi = \frac{\eta V(fC)}{k_B T} \tag{12}$$

V is the molecular volume of the rotor, η the viscosity of the medium, k_B is the Boltzmann constant, T the absolute temperature and C is a constant depending on the boundary condition. The two limiting cases for these conditions are the hydrodynamic stick and slip ones. For a non-spherical solute molecule, the value of C follows $0 < C \leq 1$. The magnitude of C depends on solute–solvent friction, and on the size of the solute relative to that the solvent molecule. The parameter f is a factor to account for the shape of the solute ($f = 1$ for a sphere, and for non-spherical molecules $f > 1$) [39]. The magnitude of the deviation from unity in the value of f indicates the degree of the non-spherical nature of the solute.

Thus, under stick- and slip-boundary condition limits, we calculated rotational times of DMAF ∼100 and ∼36 ps, respectively. The experimental value (97 ps) is close to the expected one under stick boundary conditions proposing an attachment of the solvation shell to DMAF. This result suggests that the H-bonding interactions between DMAF and DMF molecules are strong enough that the solvation shell is rotating with the solute, and this result also agrees with the observation of A emission in DMF.

For DMAF in a solution of 110 mM γ-CD, exciting at 433 nm and gating within the 470–660 nm region, a double exponential function was needed to get an accurate fit of the $r(t)$ decay. The obtained times are $\phi_1 \sim 130 \pm 20$ ps and $\phi_2 \sim 770 \pm 50$ ps. When exciting at 393 nm, we obtained ∼120 ± 20 and ∼750 ± 50 ps, respectively. The contribution of the short component changes from 79% (at 470 nm) to 86% (at 630 nm) suggesting that the observed rotational times (ϕ_1 and ϕ_2) correspond to rotors emitting at different regions. However, the change is not very large and agrees with the emission lifetime contributions (Table 1). The 130 ps rotational time is slightly longer than that of the free tautomers in DMF (97 ps). Therefore, we propose that the short component is a combination of that of A bound to CD (capped entity) and of the free DMAF structures in the bulk solvent. Note also that a rotational time of DMAF into the cavity might be as short as ∼100 ps if γ-CD does not restrict its motion, as it has been observed in other systems [9]. In fact, the results of PM3 calculations for the included *A* (Fig. 5) indicate that there is enough space between the guest and the host allowing the former to rotate with less restriction from CD. It is worth noting that the size of the included part of the DMAF (chromone moiety) is ∼5 Å, while the diameter of the larger gate of γ-CD is longer (∼9.5 Å) allowing an almost free motion of the guest.

At 110 mM of γ-CD and using the values of $K_1 = 4.1\ M^{-1}$ and $K_2 = 9.3\ M^{-1}$ we estimated ∼19% of DMAF is free, ∼31% forming inclusion complexes and ∼50% involved in the capped complexes, respectively. Thus, a small contribution of the internal rotation of the guest inside γ-CD in the short component of $r(t)$ decay seems reasonable. The longer time (770 ps) is assigned to the overall rotational time of the 1:1 inclusion complex, and its contribution is 21, 30 and 15%, when the anisotropy decay is collected at 470, 540 and 630 nm, respectively. The maximum of the contributions (30% at 540 nm) is similar to that obtained for the population of the inclusion complex using the equilibrium constants (31%).

In order to support our assignment and to get structural information on the inclusion complexes, we used the hydrodynamic theory and calculated the rotational time of these entities. The volume of inclusion complexes is much larger than that of the solvent molecules (DMF). Therefore, we took $C = 1$ and which corresponds to a stick boundary condition. To apply equation (12), the values of f and V ($4\pi abc/3$) were calculated from

the molecular dimensions of the inclusion complex optimized by PM3 method, where $a = c$ and b hold for semi major and minor axes of the ellipsoid, respectively. For the inclusion complex (C_1) $a = c = 9.4$ Å and $b = 6.9$ Å, which gives $V = 2700$ Å^3 and $f = 1.15$. Taking into account the viscosity of the solvent η (DMF at 293 K) ~ 0.80 cP, and the value of the involved parameters, we obtained $\phi(C_1) = 617$ ps, close to the corresponding experimental one (770 ps). Thus, the experimental value of ϕ corresponds to 1:1 inclusion complex. For this complex the geometry (PM3 calculations) has ~5.5 Å (phenyl amino ring) of the guest located outside the nano-cage. Finally for both free and complexed probe, the initial value of $r(t = 0) \sim 0.30$ is not far from the ideal one (0.4), a result which indicates that the emission transition moments of the complexed and free DMAF have rotated by about 24° to that of its absorption ones.

4. Conclusion

The present work shows a clear effect of γ-CD on the stabilization of complexed anion of DMAF through an intermolecular proton transfer reaction and a cooperative H-bonding network of γ-CD. Both the steady-state and ps time-resolved data show the existence of two different kinds of complexes: one in which the chromone moiety is inside the cavity (inclusion complex), and another one having the anionic molecule outside of the cavity (capped complex). The relation between the equilibrium constants for both complexes indicates that the capped complex is more stable than the inclusion one, a result in agreement with the theoretical calculations. The anisotropy measurements give the rotational times of free, complexed DMAF to CD, and of the whole DMAF:CD complexes. The data corroborate the existence of two complexes and the expected geometries by PM3 calculations. We believe that the reported results give a new insight into specific interactions of guest–host systems involving CD. The findings might be useful for the design of chemical sensors involving these nano-cavities and for drug delivery field using CD as a host [40].

Acknowledgement

This work was supported by the "Consejeria de Sanidad", the "Consejeria de Educación y Ciencia" of JCCM and MEC through projects, SAN-04-000-00, PBI-05-046 and CTQ2005-00114.

References

[1] A. Douhal, Chem. Rev. 104 (2004) 1955.
[2] N. Nandi, K. Bhattacharyya, B. Bagchi, Chem. Rev. 100 (2000) 2013.
[3] A. Douhal (Ed.), Cyclodextrin Materials Photochemistry, Photophysics and Photobiology, Elsevier, 2006.
[4] A.H. Zewail, J. Phys. Chem. A. 104 (2000) 5660.
[5] A. Douhal, T. Fiebig, M. Chachisvilis, A.H. Zewail, J. Phys. Chem. A. 102 (1998) 1657.
[6] M. Chachisvilis, I. Garcia-Ochoa, A. Douhal, A.H. Zewail, Chem. Phys. Lett. 293 (1998) 153.
[7] G. Flachenecker, P. Behrens, G. Knopp, M. Schmitt, T. Siebert, A. Vierheilig, G. Wirnsberger, A. Materny, J. Phys. Chem. A 103 (1999) 3854.
[8] J.A. Organero, L. Tormo, A. Douhal, Chem. Phys. Lett. 363 (2002) 409.
[9] J.A. Organero, A. Douhal, Chem. Phys. Lett. 373 (2003) 426.
[10] L. Tormo, A. Douhal, J. Photochem. Photobiol. A Chem. 173 (2005) 358.
[11] J. Guharay, B. Sengupta, P.K. Sengupta, Proteins 43 (2001) 75.
[12] P.K. Mandal, A. Samanta, J. Phys. Chem. A. 107 (2003) 6334.
[13] A. Banerjee, P.K. Sengupta, Chem. Phys. Lett. 424 (2006) 379.
[14] M.R. Guzzo, M. Uemi, P.M. Donate, S. Nikolaou, A.E.H. Machado, L.T. Okano, J. Phys. Chem. A 110 (2006) 10545.
[15] A. Douhal, M. Sanz, M.A. Carranza, J.A. Organero, L. Santos, Chem. Phys. Lett. 394 (2004) 54.
[16] A.D. Roshal, J.A. Organero, A. Douhal, Chem. Phys. Lett. 379 (2003) 53.
[17] P.T. Chou, M.L. Martinez, J.H. Clements, J. Phys. Chem. 97 (1993) 2618.
[18] P.-T. Chou, S.-C. Pu, W.-S. Cheng, Y.-C. Yu, F.-T. Hung, W.-P. Hu, J. Phys. Chem. A. 109 (2005) 3777.
[19] V. Shynkar, Y. Mély, G. Duportail, E. Piémont, A.S. Klymchenco, A.P. Demchenko, J. Phys. Chem. A 107 (2003) 9522.
[20] S. Ameer-Beg, S.M. Ormson, X. Poteau, R.G. Brown, P. Foggi, L. Bussotti, F.V.R. Neuwahl, J. Phys. Chem. A. 108 (2004) 6938.
[21] T.C. Swinney, D.F. Kelley, J. Chem. Phys. 99 (1993) 211.
[22] A. Sytnik, D. Gormin, M. Kasha, J. Fluoresc. 91 (1994) 11968.
[23] S.M. Ormon, R.G. Brown, F. Vollmer, W.J. Rettig, J. Photochem. Photobiol. A Chem. 81 (1994) 65.
[24] A.D. Roshal, A.V. Grigorovich, A.O. Doroshenko, V.G. Pivovarenko, A.P. Demchenko, J. Phys. Chem. A. 102 (1998) 5007.
[25] N.A. Nemkovich, W. Baumman, V.G. Pivovarenko, J. Photochem. Photobiol. A Chem. 153 (2002) 19.
[26] M. Itoh, F.M. Sumitani, K. Yoshihara, J. Phys. Chem. 90 (1986) 5672.
[27] M. Itoh, T. Yuzawa, H. Mukaihata, H. Hamaguchi, Chem. Phys. Lett. 233 (1995) 550.
[28] M.A. Smith, R.M. Neumann, R.A. Webb, J. Heterocycl. Chem. 5 (1998) 425.
[29] M.J. Frisch, et al., Gaussian 03, revision B 05, Gaussian Inc., Pittsburgh, PA, 2003.
[30] J. van Stam, S. De Feyter, F.C. De Schryver, C.H. Evans, J. Phys. Chem. 100 (1996) 19959.
[31] B. Birks, Photophysics of Aromatic Molecules, Wiley, London, 1970.
[32] A. Douhal, M. Sanz, L. Tormo, J.A. Organero, Chem. Phys. Chem. 6 (2005) 410.
[33] P. Hazra, D. Chakrabarty, A. Chakraborty, N. Sarkar, Chem. Phys. Lett. 388 (2004) 150.
[34] S.J. Strikler, R.A. Berg, J. Chem. Phys. 37 (1962) 814.
[35] R. Castro, M.J. Berardi, E. Cordova, M.O. de Olza, A.E. Kaifer, J.D. Evanseck, J. Am. Chem. Soc. 118 (1996) 10257.
[36] X.-S. Li, L. Liu, Q.-X. Guo, S.-D. Chu, Y.-C. Liu, Chem. Phys. Lett. 307 (1999) 117.
[37] F. Perrin, J. Phys. Radium, 1934.
[38] J.S. Baskin, A.H. Zewail, J. Phys. Chem. A. 105 (2001) 3680.
[39] B. Kalman, N. Clark, L.B.A. Johanson, J. Phys. Chem. 93 (1989) 4608.
[40] M. El Kemary, A. Douhal, Phochemistry and photophysics of cyclodextrin caged dugs: relevance to their stability and efficiency, in: A. Douhal (Ed.), Cyclodextrin Materials Photochemistry, Photophysics, and Photobiology, vol. 1, Elsevier, 2006, pp. 79–106, ISBN-13: 978-0-444-52780-6.